



The Open Medical Imaging Journal

Content list available at: <https://openmedicalimagingjournal.com/>



RESEARCH ARTICLE

Development of Physical Breast Phantoms for X-ray Imaging Employing 3D Printing Techniques

A. Malliori^{1,*}, A. Daskalaki¹, A. Dermitzakis¹ and N. Pallikarakis¹

¹Department of Medical Physics, Biomedical Technology Unit, Faculty of Medicine, University of Patras, Patras, Greece

Abstract:

Objective:

This study aims to investigate the use of 3D printing techniques for the fabrication of physical breast phantoms, suitable for conventional and phase contrast breast imaging. Such phantoms could provide essential information for the design, development and optimization of emerging X-ray imaging modalities.

Materials and Methods:

Physical phantoms were constructed using two 3D printing techniques: Fused Deposition Modeling and Stereolithography. Eight materials suitable for 3D printing, including thermoplastic filaments and photopolymer resins, were investigated for the optimal representation of breast tissues, based on their attenuation and refractive characteristics. The phantoms consisted of a 3D-printed mold, which was then manually filled with paraffin wax. Additionally, a 3D complex-patterned layer and details representing abnormalities were embedded in different depths. Images of the phantoms were obtained in attenuation and phase contrast mode. Experiments were conducted using an X-ray microfocus tube with Tungsten anode set to 55kVp, combined with a photon-counting detector. The distance between source and detector was 56.5cm. The images were acquired at different object-to-detector distances starting from 5cm up to 40cm in a free space propagation set-up.

Results and Conclusion:

Results show that among all combinations with paraffin used as an adipose substitute, phantoms created with the Stereolithography technique and resins (especially Flex) as glandular equivalent, were found to be more appropriate for both attenuation and phase contrast imaging. The edge enhancement effect was well observed in the experimental images acquired at 35cm object-to-detector distance, indicating the potential for improved feature visualization using this set-up in phase contrast compared to attenuation mode.

Keywords: Physical breast phantoms, 3D printing, X-ray imaging, Phase contrast, Fused deposition modeling, Stereolithography technique.

Article History

Received: December 11, 2019

Revised: February 06, 2020

Accepted: February 28, 2020

1. INTRODUCTION

Physical breast phantoms can be a valuable asset for the development, optimization and evaluation of X-ray modalities for breast imaging. Apart from quality control and testing of already existing devices, the use of physical phantoms can provide essential information for the design and development of new imaging techniques. A key factor reigniting interest in the construction of breast phantoms stems from emerging three-dimensional X-ray imaging modalities, and the need for their evaluation and further optimization. Phantoms can serve as testing objects for adjusting acquisition geometries and para-

meters, provide feedback on reconstruction algorithm accuracy, and enable image quality evaluation and dosimetric measurements. Additionally, in the final step towards clinical practice, physical phantoms can prove to be a helpful tool for better designing clinical trials, limit human involvement only to necessary and thus reduce the associated costs and extra irradiation [1, 2].

Several physical phantoms for mammography have been reported in the literature [3 - 7]. In most of them, polymethyl methacrylate (PMMA) and epoxy resins are used as suitable materials mimicking the breast tissues. A thorough review of breast phantoms for X-ray imaging, which includes both physical and computerized models (software phantoms), is reported by Glick *et al.* [8]. Most of the developed physical breast phantoms address 2D imaging, such as the Rachel

* Address correspondence to this author at the Department of Medical Physics, Biomedical Technology Unit, Faculty of Medicine, University of Patras, 26500, Rio, Patras, Greece; Tel: +30 – 2610-969109; Fax: +30 – 2610-992496; E-mail: anmall@upatras.gr

anthropomorphic phantom (Gammex 169, Gammex Inc., Middleton, WI) [7] or the TORMAX (Leeds Test Objects) [6] containing low and high contrast features surrounded by homogeneous background, while very few could be used for 3D imaging modalities. Breast Tomosynthesis (BT) is one such modality allowing pseudo-three-dimensional imaging of the breast, with a widely accepted diagnostic value [9, 10]. The influence of overlapping tissues, naturally existing in 2D mammography and possibly limiting the visibility of an abnormality, is effectively reduced in BT. Several software phantoms with a heterogeneous background suitable for BT have been investigated [11 - 16] and used for assessment and optimization studies [17 - 19]. Among the physical phantoms that have been developed, a phantom modeling of the non-uniform breast structure is the BR3D (CIRS Inc., Norfolk, VA, USA) [20]. This phantom consists of semicircular slabs with an equal thickness of 1cm and is made of two tissue-equivalent materials swirled together, corresponding to a 50/50 mixture of glandular and adipose tissue. In general, most of the commercially available physical phantoms do not reflect the heterogeneous appearance of breast tissue, nor do they have features embedded in different depths, which make their suitability as testing objects for BT highly questionable.

However, BT similarly to 2D mammography, is an imaging modality based on the attenuation of X-ray beams. Thus, in the range of energies suitable for screening, the difference in the attenuation coefficients between healthy and cancerous breasts is relatively small, resulting in poor tumor contrast. Phase contrast (PhC) imaging is an emerging technique that can enhance contrast at the boundaries of the structures due to phase shift arising from the difference in the refractive properties between the two materials [21 - 23]. This imaging technique is based not only on X-ray attenuation but also on the X-ray phase change arising from diffraction and refraction effects during X-ray scattering. Phase contrast takes place at the boundaries between materials whose refractive indices differ from each other. Tissues composed of low Z-elements, such as breast masses, produce low absorption contrast but considerable phase contrast [24, 25]. As a result, better visualization of possible abnormalities is achieved and especially in their edges, providing easier identification of lesions, characterization and finally a diagnosis. The use of PhC mode for the acquisition of BT images could combine the advantages of both techniques, producing edge-enhanced images with limited tissue overlapping. Towards this direction, a few preliminary studies using in-line (free space propagation) mode PhC tomosynthesis for imaging the breast have been conducted with simple homogeneous phantoms [26, 27], while a feasibility study including phantoms with heterogeneous texture as well was carried out by Bliznakova *et al.*, at a Synchrotron radiation facility [28]. In a recent study, conducted also at a Synchrotron facility, we have reported on the feature edge enhancement that was observed in PhC tomosynthesis images acquired using a highly heterogeneous physical phantom composed of an egg white part and lard [29]. However, PhC imaging with the use of synchrotron radiation is far from being applicable in every day clinical practice. Instead, PhC imaging employing high-resolution detectors combined with polychromatic microfocus X-ray tubes could

solve some of the practical limitations, like geometry and production of monochromatic beam [30, 31]. Photon counting detectors like Medipix have the appropriate resolution for PhC breast imaging, and therefore, motivate further studies for future clinical use [32]. Several investigations on low contrast objects were performed, showing their suitability for X-ray radiography of soft tissues and low contrast objects [33].

The progress in 3D printing brings the potential for creating low-cost breast phantoms directly from the software 3D models. Ongoing research focuses on improving printing methods and limitations concerning the precision or ability to print different materials simultaneously, but also on finding suitable mimicking materials. In the X-ray breast imaging field, there have been a few studies investigating the suitability of 3D printing materials as tissue substitutes, in terms of their attenuation coefficients in the mammographic energy range for the development of physical breast phantoms [34 - 36]. In a recent study, Ivanov *et al.* [37], investigated the suitability of seven thermoplastic polymers (ABS, Brick, Hybrid, Nylon, PET-G, PLA and PVA) and ten polymer resins (Black, Clear, Flex, Gray, NDBase, NDC+B, NDCast, NDSG, Tough, White). Attenuation coefficients and refractive index decrements of the materials were found to be in the range of 30keV to 60keV, to address the higher energies currently used in PhC [25, 38]. This study [37] showed that ABS combined with resins might be a good representation of adipose and glandular tissue for PhC imaging. Esposito *et al.* [39], focused on the investigation of the refractive index decrement of the previously mentioned 3D printed materials, with the evaluation based on the phase retrieval algorithm described by Paganin *et al.* [40]. The models used in 3D printing were created using appropriate designing software or derived from clinical images. Bucking *et al.* [41], developed printable models for ribs, liver and lung from medical imaging data and described the general workflow followed for creating a 3D printed phantom from CT images or other imaging modalities like MRI. Breast 3D printed models suitable for digital mammography, that are also based on clinical images, have been recently presented by Schopphoven *et al.* [42]. An open-source code has been introduced by Badal *et al.* [43], for the creation of such phantoms intended for 2D X-ray imaging, from printable datasets.

The 3D printing techniques can be used either for the preparation of the whole phantom directly, or partly by printing the mold and then filling it with conventional materials to build the final phantom [44]. For CT applications, simple geometric phantoms have been developed with the direct printing method [45 - 48] using different thermoplastic polymer materials or polymer resins. Moreover, phantoms with the appearance of specific organs are also reported, including the breast [49], spine [50], head [51] or even the whole body [52]. A thorough review of developed phantoms using 3D printing for different body parts and a wide range of imaging modalities (mammography, CT, MRI, PET, Ultrasound, or combinations), is reported by Filippou and Tsoumpas [44]. In a recent review, Tino *et al.* [53], focused on 3D printed phantoms for X-ray imaging and dosimetry, stressing the growing interest in 3D printing techniques, given their increasing availability and flexibility to efficiently provide customized phantoms or other

radiotherapy tools. Specifically for the breast, there are very few phantoms reported with more than one mimicking materials to represent breast tissues involving 3D printing methods. Carton *et al.* [54], followed the approach of combining 3D printed components and resins that were then manually filled in. Kiarashi *et al.* [49], developed a 3D printed breast phantom with two variations, the 'Singlet' and 'Doublet'. The latter was a phantom created using two different 3D printed materials to represent fibroglandular and adipose tissues, respectively, while the former involved only one for the fabrication of the mold and conventional materials that were then manually filled in.

Although several physical phantoms have been developed using 3D printing, very little has been done on breast imaging phantoms suitable for X-ray modalities, including both 2D mammography and advanced 3D methods like tomosynthesis with PhC. Thorough studies leading to a specialized physical phantom would enable optimization of this new imaging modality and evaluation of its potential advantages. Our group at the University of Patras has developed software tools and algorithms [11, 55 - 60] facilitating advanced X-ray breast imaging studies, including tomosynthesis and PhC and has performed simulations [18, 61, 62] and evaluation studies using a Synchrotron facility [29, 63 - 66]. In the current work, we present physical breast phantoms that can be used for further development and evaluation of such X-ray imaging modalities. Our main objective was to develop phantoms suitable for PhC imaging employing 3D printing techniques. The approach followed was to use a range of suitable 3D printable materials for the preparation of the mold, which is then filled with conventional materials, to represent fibroglandular and adipose breast tissues. Additionally, details describing breast abnormalities were embedded in different depths to allow also for tomosynthetic studies. Within our long term goal, we aim to use the developed 3D printed physical breast phantoms to perform extensive PhC tomosynthesis studies, employing high resolution photon counting detectors combined with a polychromatic microfocus X-ray tube setup.

2. MATERIALS AND METHODS

2.1. Materials

Eight materials suitable for 3D printing were investigated for the optimal representation of fibroglandular and adipose tissue, based on their attenuation and refractive characteristics. The latter needs to be considered in phantoms suitable for PhC imaging, as the amount of phase change in tissue is related to its refractive index [67]. Five of them (ABS, Hybrid, Nylon, PET-G, PLA) were thermoplastic filaments, while the other three (Clear, Flex, Tough) were photopolymer resins [1]. Their elemental composition and density are summarized in Table 1, along with the corresponding values of real breast tissues and conventional substitute materials that are commonly used for mimicking breast tissues and abnormalities in the breast.

Attenuation coefficients μ and refractive indexes δ of the studied materials are presented in Table 2, based on the data obtained in a study by Ivanov *et al.* [37] and Esposito *et al.* [39]. For breast tissues (gland and adipose), the corresponding values were derived from the National Institute of Standards

and Technology (NIST) database [68], based on elemental composition from Hammerstein *et al.* [69]. The relative difference between the linear attenuation coefficients ($\Delta\mu$) and the relative difference between the refractive decrements ($\Delta\delta$) were calculated for the studied materials, according to Eq. 1 and Eq. 2, respectively:

$$\Delta\mu_{m1,m2} = \frac{|\mu_{m1} - \mu_{m2}|}{\mu_{m2}} \times 100\% \quad (1)$$

$$\Delta\delta_{m1,m2} = \frac{|\delta_{m1} - \delta_{m2}|}{\delta_{m2}} \times 100\% \quad (2)$$

with m_1 being a testing material mimicking the gland and m_2 a material mimicking the adipose tissue. Specifically, all studied materials suitable for optimal representation of fibroglandular tissue, were further investigated with respect to paraffin as the adipose tissue equivalent.

Table 1. Elemental composition (weighted by fraction) and density for the breast tissues, conventional substitute materials (paraffin) and 3D printing materials (thermoplastic filaments and photopolymer resins).

Tissue/Material	Composition	Density (g/cm ³)
Adipose ^a	H(0.112)C(0.619)N(0.017) O(0.251) P(0.001)	0.93
Gland ^a	H(0.102)C(0.184)N(0.032)O(0.677)P(0.005)	1.04
Paraffin Wax	H(0.149)C(0.851)	0.93
ABS ^b	H(0.078)C(0.862)N(0.059)O(0.001)	1.019
Hybrid ^b	-	1.227
Nylon ^b	H(0.097)C(0.656)N(0.114)O(0.133)	1.111
PET-G ^b	H(0.052)C(0.685)N(0.012)O(0.251)	1.236
PLA ^b	H(0.058)C(0.541)N(0.018)O(0.383)	1.250
Clear ^b	H(0.085)C(0.648)N(0.059)O(0.208)	1.180
Flex ^b	H(0.087)C(0.639)N(0.044)O(0.230)	1.137
Tough ^b	-	1.181

^aData from Hammerstein *et al.* (1979).

^bData from Ivanov *et al.* (2018).

^cwww.formlabs.com/material.

2.2. Design and Phantom Implementation

The development of our physical phantoms was based on 3D printing techniques with a single material, followed by filling and solidification processes during which conventional materials were used. More precisely, the phantom consisted of a mold, created using a 3D printed material and then manually filled with paraffin wax. Paraffin wax was used as an adipose-equivalent filling material for all phantoms. Eight different 3D printing materials mentioned in Section 2.1 were investigated and used for the fabrication of the molds. These materials have close attenuation and refractive characteristics with the glandular tissue and adipose tissue. During the filling and solidification phase, features representing breast abnormalities were gradually added. Specifically, nylon spheres (3.2mm and 4.8mm), and CaCO₃ powder were added, mimicking the breast abnormalities, namely low-contrast masses and high-contrast microcalcifications (μ Cs), respectively. Before the solidification was completed, nylon fibers (0.5mm) were inserted

and an additional paraffin layer with an embedded 3D printed complex-patterned slice was superimposed on the top of some of the phantoms, to create a more heterogeneous background.

2.2.1. 3D Modeling

Our 3D models, created using the Fusion 360 and Meshmixer Autodesk software (Autodesk Inc, Computer Software, San Rafael, CA), are shown in (Fig. 1). Four different mold designs were created. Specifically, the breast phantoms were designed as semi-cylindrical of size 8,5x5cm. Two of them have 4cm thickness (Figs. 1a and 1b), one with 1cm thickness (Fig. 1c) and a thin slice with a complex pattern (Fig. 1d). The latter was used in combination with other phantoms to provide a complex heterogeneous background, while the 1cm-thick mold, printed with several materials and embedded in paraffin, enabled different combinations, providing a more dynamic phantom in terms of glandularity and thickness.

Table 2. Linear attenuation coefficient and refractive index decrement for the tissues/materials.

-	Linear Attenuation Coefficient, μ (cm^{-1})			Refractive Index, $\delta \times 10^7$		
Tissue/Material	30KeV	45KeV	60KeV	30KeV	45KeV	60KeV
Adipose ^a	0.279	0.206	0.182	2.385	1.060	0.596
Gland ^a	0.372	0.246	0.210	2.640	1.170	0.659
Paraffin Wax ^a	0.252	0.202	0.184	2.457	1.092	0.614
ABS ^b	0.273	0.210	0.189	2.534	1.126	0.633
Hybrid ^{b,c}	0.345	0.250	0.221	2.875	1.260	0.707
Nylon ^b	0.314	0.241	0.214	2.811	1.249	0.703
PET-G ^b	0.351	0.255	0.225	3.001	1.334	0.750
PLA ^b	0.439	0.286	0.244	3.059	1.360	0.765
Clear ^b	0.352	0.258	0.227	2.954	1.313	0.739
Flex ^b	0.340	0.248	0.216	2.850	1.266	0.712
Tough ^{b,c}	0.348	0.251	0.223	2.958	1.309	0.729

^aNIST.

^bData from Ivanov et al. (2018).

^cData from Esposito et al. (2019).

2.2.2. 3D Printing

Two 3D printing techniques were used for printing the selected materials: Fused Deposition Modeling (FDM) [70, 71] and Stereolithography (SLA) [72]. FDM is a simple to use and low-cost technique in terms of printers and materials used. This technique is suitable for printing thermoplastic materials, while SLA is used for printing resins. Printing time for the different printed volumes and materials used, ranged from 5h to 40h. In Table 3, temperatures for the eight investigated materials along with printing time for the 1cm-thick mold (Fig. 1c), are shown indicatively.

2.2.2.1. Printing of the Thermoplastic Materials

The five thermoplastic filaments (ABS, Hybrid, Nylon, PET-G, PLA) were printed using FDM technology with a Prusa printer (Mk3S 0.4mm nozzle HardX) of 0.1mm resolution. Among the infill patterns (grid/honeycomb/concentric/rectilinear) investigated using 100% printing density settings, the rectilinear was selected as the most

suitable to achieve the highest infill density. Before printing, all thermoplastic materials were dried for 8 hours at 85°C and placed in an industrial desiccant humidifier for an extra hour after dry. The molds were printed in flat origin, while the printer was enclosed to achieve a steady 50°C room temperature. The temperature of the nozzle for the different materials ranged from 240°C-260°C for printing the first layer and was slightly increased for the remaining layers. The temperature on the building platform was kept steady throughout the duration of printing, ranging from 85°C to 105°C, depending on the filament. Printing time ranged from 5h to 40h, for the different molds and materials used. In Table 3, temperatures and printing time are shown indicatively, for one of the printed molds (Fig. 1c) for the thermoplastic materials.

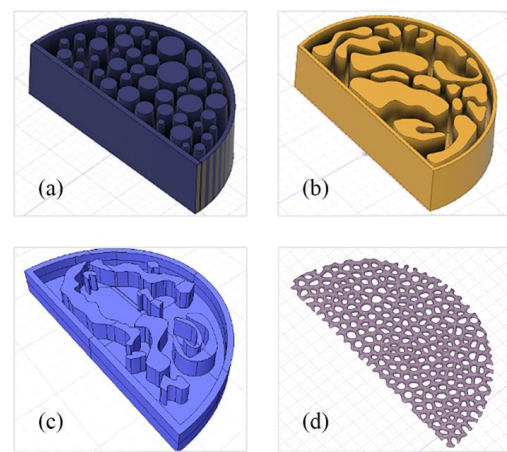


Fig. (1). The 3D models designed to be printed (a) 4cm thickness (b) 4cm thickness (c) 1cm thickness and (d) the thin complex-patterned layer.

Table 3. Printing time and temperature for the 3D printing materials used (thermoplastic filaments and photopolymer resins).

Material	Printing Technique	Build Volume	Printing Time (h)	Temperature (°C)
ABS	FDM	85x50x10mm	6 at max 40mm/sec	250 ^f / 255 ^r / 100 ^p
Hybrid	FDM	85x50x10mm	5 at max 40mm/sec	260 ^f / 265 ^r / 105 ^p
Nylon	FDM	85x50x10mm	5 at max 40mm/sec	260 ^f / 260 ^r / 105 ^p
PET-G	FDM	85x50x10mm	5 at max 40mm/sec	245 ^f / 250 ^r / 85 ^p
PLA	FDM	85x50x10mm	4.5 at max 40mm/sec	215 ^f / 220 ^r / 85 ^p
Clear	SLA	30ml ^s / 16ml ^w	4.5 ^s / 1.5 ^w	31
Flex	SLA	30ml ^s / 16ml ^w	8 ^s / 3.5 ^w	33
Tough	SLA	30ml ^s / 16ml ^w	6.5 ^s / 2.5 ^w	35

^ffirst layer.

^rremaining layers.

^pbuild plate.

^swith supports.

^wwithout supports.

2.2.2.2. Printing of the Polymer Resins

The three resins (Clear, Flex and Tough) were printed using SLA technology with a Formlabs Form 2 (140 μm focus spot size, 100 μm vertical resolution). Printing fill density was set to 100% and the procedure involved an Isopropyl Alcohol (IPA) bath followed by UV curing. The 4cm-thick molds were initially printed upside down with supports. However, poor printing quality was observed, therefore the approach that was finally followed, was to print the molds directly on the platform with a small hole to avoid pressure-induced forces. The temperature for the different materials ranged from 31°C to 33°C, while the printing times ranged from 5h to 15h for the different molds and materials used. Temperatures and printing times for the three polymer resins are also shown indicatively in Table 3 for one of the printed molds (Fig. 1c).

2.2.3. Filling with Paraffin and Solidification

Paraffin was heated up to 70°C and then poured into the empty spaces of the molds. During the filling and solidification process, the features of interest (nylon spheres, nylon fibers and CaCO₃ powder) were gradually added. Before the solidification was completed, the additional paraffin layer with a 3D complex-patterned slice embedded (Fig. 1d) was superimposed on top of some of the phantoms. Fig. (2) shows Regions of Interest (ROIs) of the printed molds for all the investigated materials. Images of the physical phantoms during the different steps of the process are shown in Fig. (3).

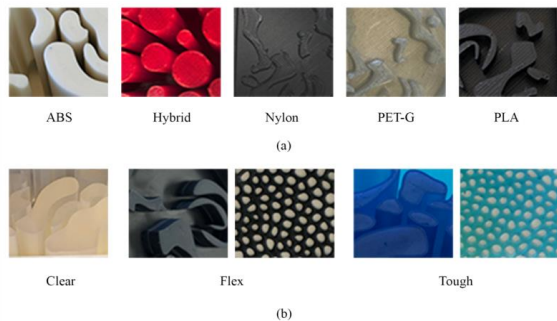


Fig. (2). ROIs of the printed molds for all the investigated materials (a) the five thermoplastic materials (ABS, Hybrid, Nylon, PET-G, PLA) printed with FDM technique and (b) the three polymer resins (Clear, Flex and Tough) printed with SLA technique.

The phantoms were left up to 10 hours for slow solidification in room temperature conditions. Images depicting the different phases of the process during phantom construction are shown in Fig. (3).

2.3. Image Acquisition

The experiments for attenuation and phase sensitive imaging were carried out at the Institute of Experimental and Applied Physics at Czech Technical University in Prague. The table-top set up illustrated in Fig. (4), was based on a 150kV X-ray microfocus tube with Tungsten anode (Hamamatsu L12161-07) and focal spot size 5 μm . The microfocus tube was combined with a 300 μm Si multi-chip detector array bumb-

bonded (4x5 Timepix chips of 256x256 square pixel matrix and pixel pitch of 55 μm) producing images of 1280x1024 pixels. The phantoms were placed on a metal plate moving horizontally between the source and the detector, producing images of different magnifications. In this set-up, planar images can be acquired as in 2D mammography, while the plate can also rotate up to 360° enabling BT studies as well. The distance between the source and the detector (SDD) was 56.5cm. The images were acquired at the different object to detector distances (ODD) starting from 5cm up to 40cm in a free space propagation set up. Small ODDs produced images sensitive in attenuation contrast, whereas ODDs higher than 30 cm produced images where phase contrast effects contributed, referred in the text as attenuation and phase contrast imaging, respectively. The source was set to 55kVp and 111mAs with the use of a 200 μm Al filter.

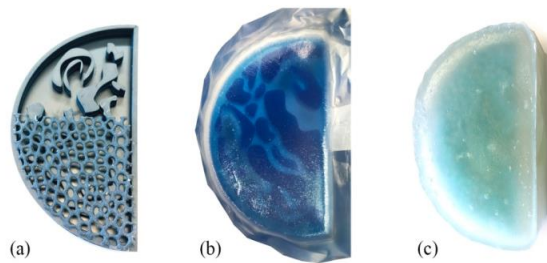


Fig. (3). Images of the physical phantoms during different stages of construction: (a) 3D printing of the molds and the complex-patterned layer (b) Filling process of the molds with paraffin embedding details simulating abnormalities (c) Solidification of the phantom. The complex-patterned layer can be seen on the top of the phantom embedded in paraffin.

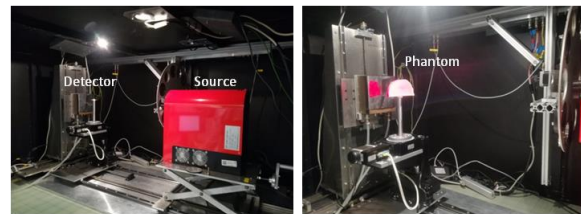


Fig. (4). Table-top set up of the experiments where the microfocus X-ray tube, the detector and the placement of the phantom are illustrated.

The images were post-processed by applying flat field/beam hardening corrections in order to avoid streak artifacts taking into account the signal-to-thickness equivalent correction [73 - 75].

3. RESULTS

The following graphs show the difference in the linear attenuations ($\Delta\mu_{mi,paraffin}$) and refractive index decrements ($\Delta\delta_{mi,paraffin}$) at photon energies 30 keV, 45 keV and 60 keV, for all the investigated materials with respect to the paraffin, as calculated from Eq. (1) and Eq. (2) (Section 2.1). The values ($\Delta\mu_{gland,adipose}$) and ($\Delta\delta_{gland,adipose}$) were also calculated for these energies and are presented in the graphs with the dotted lines.

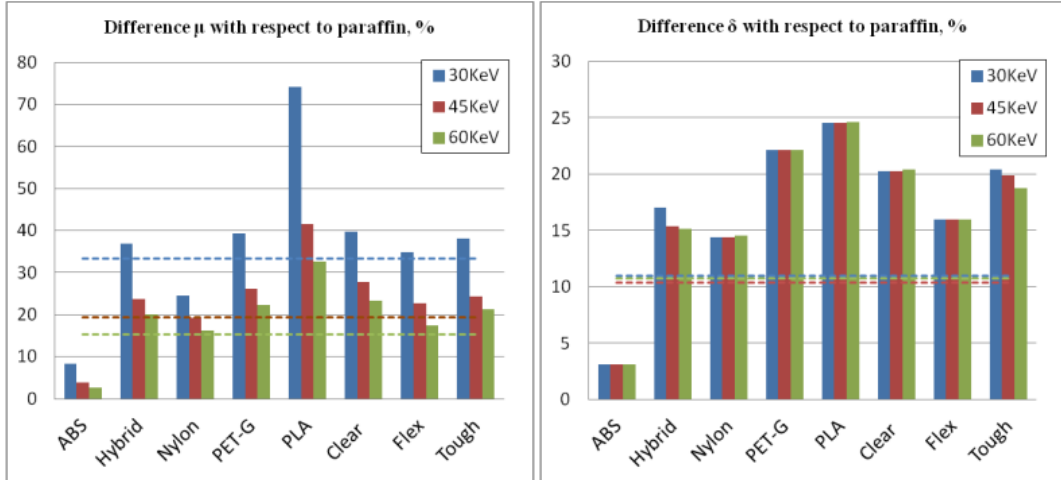


Fig. (5). Difference % in μ (on the left) and δ (on the right) for the selected 3D printing materials with respect to paraffin at 30 keV, 45keV and 60keV. Dotted lines present the values $\Delta\mu_{\text{gland,adipose}}$ and $\Delta\delta_{\text{gland,adipose}}$ for the same energies.

In Fig. (6), some tomographic slices of the phantoms created following the procedure described in Section 2.2, are shown indicatively. In the first column, Figs. (6a and 6c) correspond to the 3D models presented in Figs. (1b and 1c), respectively. In the second column, Fig. (6b and 6d) show two different slices depicting the complex background created from the combination of one of these models (Fig. 1b) with the complex-patterned layer (Fig. 1d).

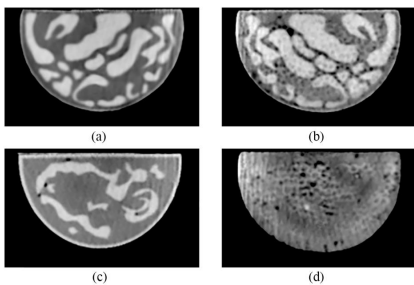


Fig. (6). Tomographic slices of created phantoms without the complex layer (first column) and with the complex layer embedded (second column).

In Fig. (7), ROIs focusing on the inserted features of interest are depicted. Specifically Fig. (7a) shows the radiographic appearance of CaCO_3 specs mimicking a cluster of high-contrast microcalcifications, while Fig. (7b) shows a nylon sphere of 3,2mm representing a low-contrast mass.

In Fig. (8), ROIs of planar images from the phantoms are presented. These images were acquired from phantoms with different combinations of paraffin/resin materials (row a) clear, b) tough and c) flex), at two ODDs 5cm (column i) and 35cm (column ii). In the first column, images based on the attenuation contrast are illustrated, whereas in the second column phase contrast effects contribute to the images. Also in the ROIs of Figs. (8b and 8c), the nylon spheres representing breast masses that were embedded into the base material (paraffin) of the phantoms, are depicted.

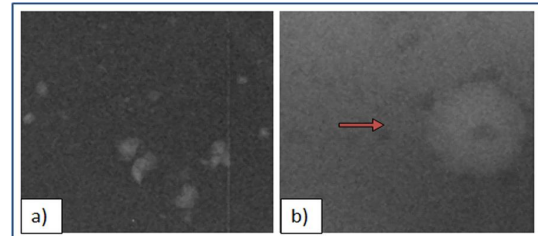


Fig. (7). Features of interest mimicking breast abnormalities a) CaCO_3 specs representing a cluster of microcalcifications b) nylon sphere (3.2mm) representing a mass.

ROIs	ODD=5cm	ODD=35cm
a) SLA / Clear	i	ii
b) SLA / Tough		
c) SLA / Flex		

Fig. (8). ROIs of planar images acquired at ODD 5cm (column i) and ODD 35cm (column ii) from the phantoms with resins, a) Clear, b) Tough and c) Flex.

Similarly, in Fig. (9) ROIs of the images acquired from phantoms with different combinations of paraffin/thermoplastic materials (row a) PET-G, (row b) Nylon, (row c) ABS and (row d) Hybrid at two ODDs, 5cm (column i) and 35cm (column ii) are presented. The two ROIS Figs. (9b and 9c) focus on the low-contrast masses, while Fig. (9a) shows the nylon fiber.

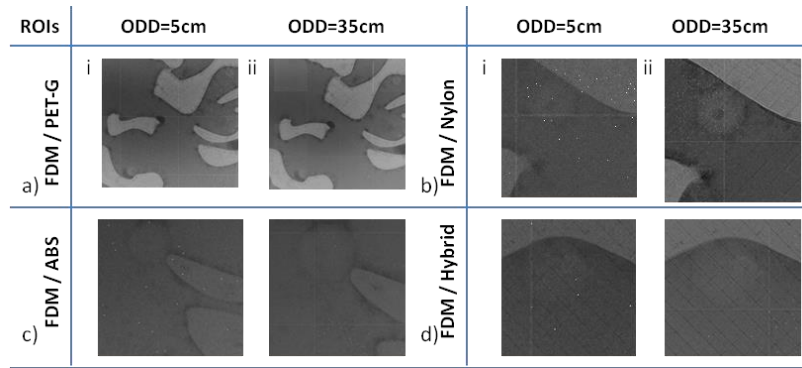


Fig. (9). ROIs of planar images acquired at ODD 5cm (column i) and ODD 35cm (column ii) from the phantoms with thermoplastic materials, **a)** PET-G, **b)** Nylon, **c)** ABS and **d)** Hybrid.

4. DISCUSSION

The presented physical breast phantoms were created by employing 3D printing techniques and are suitable for conventional and X-ray PhC imaging. For the development of phantoms, a single 3D printed material was used for the creation of the mold, followed by a filling process with paraffin-wax and embedded features of interest. A similar approach was followed by Kiarashi *et al.* [49], for the construction of the 'Singlet' phantom, which was fabricated using a glandular-equivalent 3D printed material and then carefully filled with adipose-equivalent materials (oil, beeswax and a permanent resin) for investigation. In our case, paraffin wax was used as the chosen adipose-equivalent material for all phantoms, while eight 3D printed materials, including both thermoplastics and resins, were investigated to simulate the glandular tissue. Spherical low-contrast lesions (referred as masses) and clusters of high-contrast microcalcifications were considered as the main features of interest, similarly to most commercially available mammography phantoms used for image quality assessment.

The substitute materials used for the creation of the phantoms were selected to mimic both the attenuation and refractive properties of the breast. Thus, the developed phantoms can be used in X-ray PhC applications allowing testing of this modality. More precisely, the phantom could be used for the optimization of reconstruction algorithms, acquisition geometries and parameters potentially leading to superior detectability and visibility of breast lesions. The different combinations with the complex pattern slice that are possible (Figs. 6b and 6d) could result in a tissue-equivalent breast phantom with a heterogeneous background with dynamic thickness and glandularity that could be adapted to the needs, suitable for both 2D and BT studies.

Concerning the construction of the molds, two 3D printing techniques were employed following the procedures analytically described in sections 2.2.2.1 and 2.2.2.2. The rectilinear pattern was chosen in the FDM technique, to produce better infill density and the thermoplastic materials were dried before printing to avoid moisture absorbance preserving the printing quality. In SLA, the approach followed to make a small hole on the mold, served to avoid pressure-

induced forces and improved the printing quality. As shown in Fig. (3), high printing quality was achieved in the molds, with solid and smooth surfaces, especially for the case of the resins printed with SLA. However, in some of the phantoms areas, small air bubbles were observed in the obtained images. These air bubbles are visible in the phantoms shown in Figs. (6b, 6c, 6d) indicatively and were created during the filling process and the manual insertion of features of interest. The formation of such air cavities is undesirable and could be possibly eliminated using a vacuum chamber during the procedure, to avoid air getting trapped inside. Overall, 3D printing brings the potential to create reproducible low-cost phantoms enabling custom designs that can be printed directly from the 3D models. However, there are also limitations mainly related to factors stemming from the current 3D printing technology status, such as an inability to print multiple materials at the same time.

Investigated 3D printed materials were considered in combination with paraffin as the adipose-tissue substitute Fig. (5). All three resins (Clear, Flex and Tough) are suitable and were investigated as glandular substitutes. Among thermoplastic filaments, ABS has a μ value closer to adipose tissues, while the rest could be used as glandular equivalents. Based on the relative differences in both μ and δ , among all combinations with paraffin being used as the adipose substitute, Flex-Paraffin, Nylon-Paraffin and Hybrid-Paraffin were the optimal combinations for the representation of the glandular and adipose tissues, regarding their attenuation and refractive characteristics. The PhC effect was well detected in images obtained with the created phantoms for both resins (Fig. 8) and thermoplastic filaments (Fig. 9).

The comparison between the two columns in Fig. (8) shows that the edges and the contrast of the structures enhanced in the case of higher ODD (column ii), where PhC effects contributed to the image. In Fig. (8b), the sphere can be better visualized for 35cm ODD, where it appears with sharper edges due to the PhC effect, compared to 5cm ODD. The same stands for the spheres in Fig. (8c), where the small one is hardly detected for the case of 5cm ODD. The enhanced contrast of low contrast features such as breast masses remains one of the most important goals of breast imaging and a crucial

matter for early detection of breast cancer [76]. Moreover, breast masses are categorized according to their shape and margins [77], so enhanced visualization of their borders is essential. Similarly, in Fig. (9), the low contrast features (spheres and fibers) are better visualized at ODD=35cm for all phantoms due to the PhC effect. The spheres in Figs. (9b and 9c) are characteristic examples, that appear with enhanced resolution of their edges at ODD=35cm. It is worth mentioning that in Fig. (9a) (ii) the nylon fiber is detected due to the PhC effect, whereas for smaller ODDs, it could not be distinguished among the paraffin background.

Visual assessment between the images of the phantoms created using the two different 3D printing techniques FDM and SLA, indicates that the latter proves to be more appropriate for the development of breast phantoms. As observed in Fig. (9) from the images of the phantoms constructed with FDM, the printing patterns are visible, resulting in a rippled and rough surface. This drawback is more evident for Nylon and Hybrid Figs. (9b and 9d). Also, even though the infill density was chosen to be 100%, hollow areas remained in the construction of the molds depicted in the images as black areas. This disadvantage for breast imaging becomes even stronger and unpleasant in the case of PhC, where the edge enhancement takes place (and the printing pattern results in strong artifacts). On the contrary, despite being a more expensive technique, SLA provided rigid and smoother areas with better surface finish (Fig. 8). To sum up, the air cavities and printing artifacts are unwanted in X-ray breast phantoms, especially for PhC imaging, which indicate that SLA and thus the phantoms with molds printed with the three resins (Flex, Clear, Tough) could be considered as more suitable.

CONCLUSION

The presented study showed that 3D printing techniques can be used for developing complex breast tissue-mimicking phantoms that are suitable for the investigation of multiple X-ray imaging modalities with the same phantom. The investigated techniques produced phantoms that could be used for 2D or 3D imaging techniques, in both attenuation and phase contrast based X-ray mode. Among the different materials and printing techniques investigated, Flex-Paraffin, Nylon-Paraffin and Hybrid-Paraffin were found to be the most suitable choices for mimicking breast tissues, while SLA proved to be more appropriate for the development of breast phantoms giving the resins as substitute materials the lead. Contrary to SLA, FDM produced visible printing patterns resulting in a rippled and rough surface that deteriorated the quality of the acquired X-ray images. The developed physical breast phantoms were imaged using a polychromatic micro-focus X-ray tube setup, in order to investigate the presence of PhC effect. Results showed that the PhC effect was present even in ODD of 35cm, rendering the imaging setup suitable for PhC imaging and therefore overcoming one of the main limitations for clinical use of PhC imaging, imposed by synchrotron-based in-line setups.

ETHICS APPROVAL AND CONSENT TO PARTICIPATE

Not applicable.

HUMAN AND ANIMAL RIGHTS

No animals/humans were used for studies that are the basis of this research.

CONSENT FOR PUBLICATION

Not applicable.

AVAILABILITY OF DATA AND MATERIALS

Not applicable.

FUNDING

This research is implemented through the Operational Program “Human Resources Development, Education and Lifelong Learning” and is co-financed by the European Union (European Social Fund) and Greek national funds.

CONFLICT OF INTEREST

The author declares no conflict of interest, financial or otherwise.

ACKNOWLEDGEMENTS

The experiments were carried out at the Institute of Experimental and Applied Physics at Czech Technical University in Prague under the guidance of Dr. Martin Pichotka. The authors would also like to thank Dr. Jan Dudak and Dr. Jan Zemlicka for their advice.

REFERENCES

- [1] Young S, Bakic PR, Myers KJ, Jennings RJ, Park S. A virtual trial framework for quantifying the detectability of masses in breast tomosynthesis projection data. *Med Phys* 2013; 40(5): 051914. [<http://dx.doi.org/10.1118/1.4800501>] [PMID: 23635284]
- [2] Kiarashi N, Lo JY, Lin Y, et al. Development and application of a suite of 4-D virtual breast phantoms for optimization and evaluation of breast imaging systems. *IEEE Trans Med Imaging* 2014; 33(7): 1401-9. [<http://dx.doi.org/10.1109/TMI.2014.2312733>] [PMID: 24691118]
- [3] Destouet JM, Bassett LW, Yaffe MJ, Butler PF, Wilcox PA. The ACR's Mammography Accreditation Program: Ten years of experience since MQSA. *J Am Coll Radiol* 2005; 2(7): 585-94. [<http://dx.doi.org/10.1016/j.jacr.2004.12.005>] [PMID: 17411883]
- [4] ACR. New ACR digital mammography quality control manual <https://www.acr.org/>
- [5] Bijkerk K, Lindeijer J, Thijssen M. The CDMAM phantom: A contrast-detail phantom specifically for mammography. *Radiology* 1993; 185: 395.
- [6] TOR MAX Phantom. <https://www.leedstestobjects.com/index.php/phantom/tor-max/>
- [7] Caldwell CB, Yaffe MJ. Development of an anthropomorphic breast phantom. *Med Phys* 1990; 17(2): 273-80. [<http://dx.doi.org/10.1118/1.596506>] [PMID: 2333054]
- [8] Glick SJ, Ikejimba LC. Advances in digital and physical anthropomorphic breast phantoms for x-ray imaging. *Med Phys* 2018; 45(10): e870-85. [<http://dx.doi.org/10.1002/mp.13110>] [PMID: 30058117]
- [9] Sechopoulos I. A review of breast tomosynthesis. Part I. The image acquisition process. *Med Phys* 2013; 40(1): 014301. [<http://dx.doi.org/10.1118/1.4770279>] [PMID: 23298126]
- [10] Vedantham S, Karella S, Vijayaraghavan GR, Kopans DB. Digital breast tomosynthesis: State of the art. *Radiology* 2015; 277(3): 663-84. [<http://dx.doi.org/10.1148/radiol.2015141303>] [PMID: 26599926]
- [11] Bliznakova K, Bliznakov Z, Bravou V, Kolitsi Z, Pallikarakis N. A three-dimensional breast software phantom for mammography simulation. *Phys Med Biol* 2003; 48(22): 3699-719. [<http://dx.doi.org/10.1088/0031-9155/48/22/006>] [PMID: 14680268]
- [12] Bliznakova K, Suryanarayanan S, Karella S, Pallikarakis N.

- Evaluation of an improved algorithm for producing realistic 3D breast software phantoms: Application for mammography. *Med Phys* 2010; 37(11): 5604-17.
[\[http://dx.doi.org/10.1118/1.3491812\]](http://dx.doi.org/10.1118/1.3491812) [PMID: 21158272]
- [13] Bakic PR, Zhang C, Maidment AD. Development and characterization of an anthropomorphic breast software phantom based upon region-growing algorithm. *Med Phys* 2011; 38(6): 3165-76.
[\[http://dx.doi.org/10.1118/1.3590357\]](http://dx.doi.org/10.1118/1.3590357) [PMID: 21815391]
- [14] Carton AK, Grisey A, Carvalho P, Dromain C, Muller S. A virtual human breast phantom using surface meshes and geometric internal structures. 2014.
[\[http://dx.doi.org/10.1007/978-3-319-07887-8_50\]](http://dx.doi.org/10.1007/978-3-319-07887-8_50)
- [15] Elangovan P, Mackenzie A, Dance DR, et al. Design and validation of realistic breast models for use in multiple alternative forced choice virtual clinical trials. *Phys Med Biol* 2017; 62(7): 2778-94.
[\[http://dx.doi.org/10.1088/1361-6560/aa622c\]](http://dx.doi.org/10.1088/1361-6560/aa622c) [PMID: 28291738]
- [16] Li Z. Task-based optimization of 3D breast x-ray imaging using mathematical observers. 2017.
- [17] Bakic P, Ng S, Ringer P, Carton AK, Conant E, Maidment A. Validation and optimization of digital breast tomosynthesis reconstruction using an anthropomorphic software breast phantom. *SPIE Medical Imaging* 2010; p. 7622.
[\[http://dx.doi.org/10.1117/12.845299\]](http://dx.doi.org/10.1117/12.845299)
- [18] Malliori A, Bliznakova K, Sechopoulos I, Kamarianakis Z, Fei B, Pallikarakis N. Breast tomosynthesis with monochromatic beams: A feasibility study using Monte Carlo simulations. *Phys Med Biol* 2014; 59(16): 4681-96.
[\[http://dx.doi.org/10.1088/0031-9155/59/16/4681\]](http://dx.doi.org/10.1088/0031-9155/59/16/4681) [PMID: 25082791]
- [19] Zeng R, Badano A, Myers KJ. Optimization of digital breast tomosynthesis (DBT) acquisition parameters for human observers: Effect of reconstruction algorithms. *Phys Med Biol* 2017; 62(7): 2598-611.
[\[http://dx.doi.org/10.1088/1361-6560/aa5ddc\]](http://dx.doi.org/10.1088/1361-6560/aa5ddc) [PMID: 28151728]
- [20] CIRS BR3D BREAST IMAGING PHANTOM. <https://www.cirsinc.com/products/mammography/br3d-breast-imaging-phantom/>
- [21] Castelli E, Tonutti M, Arfelli F, et al. Mammography with synchrotron radiation: First clinical experience with phase-detection technique. *Radiology* 2011; 259(3): 684-94.
[\[http://dx.doi.org/10.1148/radiol.11100745\]](http://dx.doi.org/10.1148/radiol.11100745) [PMID: 21436089]
- [22] Bravin A, Coan P, Suortti P. X-ray phase-contrast imaging: From pre-clinical applications towards clinics. *Phys Med Biol* 2013; 58(1): R1-R35.
[\[http://dx.doi.org/10.1088/0031-9155/58/1/R1\]](http://dx.doi.org/10.1088/0031-9155/58/1/R1) [PMID: 23220766]
- [23] Wu X, Liu H. Clinical implementation of x-ray phase-contrast imaging: Theoretical foundations and design considerations. *Med Phys* 2003; 30(8): 2169-79.
[\[http://dx.doi.org/10.1118/1.1593836\]](http://dx.doi.org/10.1118/1.1593836) [PMID: 12945983]
- [24] Olivo A, Rigon L, Vinnicombe SJ, Cheung KC, Ibison M, Speller RD. Phase contrast imaging of breast tumours with synchrotron radiation. Applied radiation and isotopes : Including data, instrumentation and methods for use in agriculture, industry and medicine 2009; 67(6): 1033-41.
[\[http://dx.doi.org/10.1016/j.apradiso.2009.01.075\]](http://dx.doi.org/10.1016/j.apradiso.2009.01.075)
- [25] Sarno A, Mettivier G, Golosio B, Oliva P, Spandre G, Di Lillo F, et al. Imaging performance of phase-contrast breast computed tomography with synchrotron radiation and a CdTe photon-counting detector. *Physica medica : PM : An international journal devoted to the applications of physics to medicine and biology : Official journal of the Italian Association of Biomedical Physics* 2016; 32(5): 681-90.
[\[http://dx.doi.org/10.1016/j.ejmp.2016.04.011\]](http://dx.doi.org/10.1016/j.ejmp.2016.04.011)
- [26] Guan H, Xu Q, Garson A, Anastasio M. Depth resolution properties of in-line X-ray phase-contrast tomosynthesis. *SPIE Medical Imaging* 2014; p. 9033.
- [27] Hammonds JC, Price RR, Donnelly EF, Pickens DR. Phase-contrast digital tomosynthesis. *Med Phys* 2011; 38(5): 2353-8.
[\[http://dx.doi.org/10.1118/1.3574871\]](http://dx.doi.org/10.1118/1.3574871) [PMID: 21776769]
- [28] Bliznakova K, Russo P, Kamarianakis Z, et al. In-line phase-contrast breast tomosynthesis: A phantom feasibility study at a synchrotron radiation facility. *Phys Med Biol* 2016; 61(16): 6243-63.
[\[http://dx.doi.org/10.1088/0031-9155/61/16/6243\]](http://dx.doi.org/10.1088/0031-9155/61/16/6243) [PMID: 27486086]
- [29] Daskalaki A, Malliori A, Dermitsaklis A, Pallikarakis N. Novel physical heterogeneous breast phantom for x-ray phase contrast imaging. *Badnjevic, A, Škrbić, R, Gurbeta Pokvić, L (eds) CMBEBIH (2019) IFMBE Proceedings*. Springer, Cham. 2019; pp. 73: 105-10.
- [30] Procz S, Avila C, Fey J, Roque G, Schuetz M, Hamann E. X-ray and gamma imaging with Medipix and Timepix detectors in medical research. *Radiat Meas* 2019; 127106104
[\[http://dx.doi.org/10.1016/j.radmeas.2019.04.007\]](http://dx.doi.org/10.1016/j.radmeas.2019.04.007)
- [31] Pichotka M, Palma K, Hasn S, Jakubek J, Vavrik D. Experimentally enhanced model-based deconvolution of propagation-based phase-contrast data. *J Instrum* 2016; 11(12): C12037.
[\[http://dx.doi.org/10.1088/1748-0221/11/12/C12037\]](http://dx.doi.org/10.1088/1748-0221/11/12/C12037)
- [32] Palma KD, Pichotka M, Hasn S, Granja C. Table-top phase-contrast imaging employing photon-counting detectors towards mammographic applications. *J Instrum* 2017; 12(02): C02032.
[\[http://dx.doi.org/10.1088/1748-0221/12/02/C02032\]](http://dx.doi.org/10.1088/1748-0221/12/02/C02032)
- [33] Jakubek J, Granja C, Dammer J, Hanus R, Holy T, Pospisil S, et al. Phase contrast enhanced high resolution X-ray imaging and tomography of soft tissue. *Nucl Instrum Methods Phys Res A* 2007; 571(1): 69-72.
[\[http://dx.doi.org/10.1016/j.nima.2006.10.031\]](http://dx.doi.org/10.1016/j.nima.2006.10.031)
- [34] Clark M, Ghamraoui B, Badal A. Reproducing 2D breast mammography images with 3D printed phantoms. *Proc SPIE, Physics of Medical Imaging*. 9783.
- [35] Sikaria D, Musinksy S, Sturgeon G, Solomon J, Dia A, Gehm M, et al. Second Generation Anthropomorphic Physical Phantom for Mammography and DBT: Incorporating Voxelized 3D Printing and Inkjet Printing of Iodinated Lesion Inserts. *Proc SPIE: Physics of Medical Imaging*. 9783.
- [36] Zhao C, Solomon JGS, Gehm M, Catenacci M, Wiley B, et al. Thrid generation anthropomorphic physical phantom for mammography and DBT: Incorporating voxelized 3D printing and uniform chest wall QC region. *Proc SPIE, Physics of Medical Imaging*. 10132.
- [37] Ivanov D, Bliznakova K, Buliev I, et al. Suitability of low density materials for 3D printing of physical breast phantoms. *Phys Med Biol* 2018; 63(17): 175020.
[\[http://dx.doi.org/10.1088/1361-6560/aad315\]](http://dx.doi.org/10.1088/1361-6560/aad315) [PMID: 29999497]
- [38] Ghani MU, Wong MD, Omoumi FH, Zheng B, Fajardo LL, Yan A, et al. Detectability comparison of simulated tumors in digital breast tomosynthesis using high-energy X-ray inline phase sensitive and commercial imaging systems *Physica medica : PM : An international journal devoted to the applications of physics to medicine and biology: Official journal of the Italian Association of Biomedical Physics* 2018; 47: 34-41.
- [39] Esposito G, Mettivier G, Bliznakova K, et al. Investigation of the refractive index decrement of 3D printing materials for manufacturing breast phantoms for phase contrast imaging. *Phys Med Biol* 2019; 64(7)075008
[\[http://dx.doi.org/10.1088/1361-6560/ab0670\]](http://dx.doi.org/10.1088/1361-6560/ab0670) [PMID: 30754030]
- [40] Paganin D, Mayo SC, Gureyev TE, Miller PR, Wilkins SW. Simultaneous phase and amplitude extraction from a single defocused image of a homogeneous object. *J Microsc* 2002; 206(Pt 1): 33-40.
[\[http://dx.doi.org/10.1046/j.1365-2818.2002.01010.x\]](http://dx.doi.org/10.1046/j.1365-2818.2002.01010.x) [PMID: 12000561]
- [41] Bücking TM, Hill ER, Robertson JL, Maneas E, Plumb AA, Nikitichev DI. From medical imaging data to 3D printed anatomical models. *PLoS One* 2017; 12(5): e0178540.
[\[http://dx.doi.org/10.1371/journal.pone.0178540\]](http://dx.doi.org/10.1371/journal.pone.0178540) [PMID: 28562693]
- [42] Schopphoven S, Cavael P, Bock K, Fiebich M, Mäder U. Breast phantoms for 2D digital mammography with realistic anatomical structures and attenuation characteristics based on clinical images using 3D printing. *Phys Med Biol* 2019; 64(21): 215005.
[\[http://dx.doi.org/10.1088/1361-6560/ab3f6a\]](http://dx.doi.org/10.1088/1361-6560/ab3f6a) [PMID: 31469105]
- [43] Badal A, Clark M, Ghamraoui B. Reproducing two-dimensional mammograms with three-dimensional printed phantoms. *J Med Imaging (Bellingham)* 2018; 5(3): 033501.
[\[http://dx.doi.org/10.1117/1.JMI.5.3.033501\]](http://dx.doi.org/10.1117/1.JMI.5.3.033501) [PMID: 30035152]
- [44] Filippou V, Tsoumpas C. Recent advances on the development of phantoms using 3D printing for imaging with CT, MRI, PET, SPECT, and ultrasound. *Med Phys* 2018.
[\[http://dx.doi.org/10.1002/mp.13058\]](http://dx.doi.org/10.1002/mp.13058) [PMID: 29933508]
- [45] Solomon J, Ba A, Bochud F, Samei E. Comparison of low-contrast detectability between two CT reconstruction algorithms using voxel-based 3D printed textured phantoms. *Med Phys* 2016; 43(12): 6497.
[\[http://dx.doi.org/10.1118/1.4967478\]](http://dx.doi.org/10.1118/1.4967478) [PMID: 27908164]
- [46] Dancewicz OL, Sylvander SR, Markwell TS, Crowe SB, Trapp JV. Radiological properties of 3D printed materials in kilovoltage and megavoltage photon beams *Physica medica : PM : An international journal devoted to the applications of physics to medicine and biology: Official journal of the Italian Association of Biomedical Physics* 2017; 38: 111-8.
- [47] Seong Y. Evaluation of usefulness for quality control phantom of computed tomography produced by using fused deposition modeling

- 3d printing technology. *J Eng Appl Sci (Asian Res Publ Netw)* 2017; 12: 3137-41.
- [48] Shin J, Sandhu RS, Shih G. Imaging properties of 3d printed materials: Multi-Energy CT of filament polymers. *J Digit Imaging* 2017; 30(5): 572-5. [http://dx.doi.org/10.1007/s10278-017-9954-9] [PMID: 28168529]
- [49] Kiarashi N, Nolte AC, Sturgeon GM, et al. Development of realistic physical breast phantoms matched to virtual breast phantoms based on human subject data. *Med Phys* 2015; 42(7): 4116-26. [http://dx.doi.org/10.1118/1.4919771] [PMID: 26133612]
- [50] Javan R, Bansal M, Tangestanipoor A. A prototype hybrid gypsum-based 3-dimensional printed training model for computed tomography-guided spinal pain management. *J Comput Assist Tomogr* 2016; 40(4): 626-31. [http://dx.doi.org/10.1097/RCT.0000000000000415] [PMID: 27434789]
- [51] Kamomae T, Shimizu H, Nakaya T, Okudaira K, Aoyama T, Oguchi H, et al. Three-dimensional printer-generated patient-specific phantom for artificial *in vivo* dosimetry in radiotherapy quality assurance. *Physica medica : PM : An international journal devoted to the applications of physics to medicine and biology: Official journal of the Italian Association of Biomedical Physics* 2017; 44: 205-11. [http://dx.doi.org/10.1016/j.ejmp.2017.10.005]
- [52] Lee MY, Han B, Jenkins C, Xing L, Suh TS. A depth-sensing technique on 3D-printed compensator for total body irradiation patient measurement and treatment planning. *Med Phys* 2016; 43(11): 6137. [http://dx.doi.org/10.1118/1.4964452] [PMID: 27806603]
- [53] Tino R, Yeo A, Leary M, Brandt M, Kron T. A systematic review on 3d-printed imaging and dosimetry phantoms in radiation therapy. *Technol Cancer Res Treat* 2019; 181533033819870208. [http://dx.doi.org/10.1177/1533033819870208] [PMID: 31514632]
- [54] Carton AK, Bakic P, Ullberg C, Derand H, Maidment AD. Development of a physical 3D anthropomorphic breast phantom. *Med Phys* 2011; 38(2): 891-6. [http://dx.doi.org/10.1118/1.3533896] [PMID: 21452726]
- [55] Kolitsi Z, Panayiotakis G, Anastassopoulos V, Scodras A, Pallikarakis N. A multiple projection method for digital tomosynthesis. *Med Phys* 1992; 19(4): 1045-50. [http://dx.doi.org/10.1118/1.596822] [PMID: 1518466]
- [56] Lazos D, Bliznakova K, Kolitsi Z, Pallikarakis N. An integrated research tool for X-ray imaging simulation. *Comput Methods Programs Biomed* 2003; 70(3): 241-51. [http://dx.doi.org/10.1016/S0169-2607(02)00015-9] [PMID: 12581556]
- [57] Bliznakova K, Sechopoulos I, Buliev I, Pallikarakis N. BreastSimulator: A software platform for breast x-ray imaging research. *J Biomed Graph Comput* 2012; 2(1): 1-14. [http://dx.doi.org/10.5430/jbgc.v2n1p1]
- [58] Malliori A, Bliznakova K, Daskalaki A, Pallikarakis N. Graphical User Interface for Breast Tomosynthesis Reconstructions: An Application Using Anisotropic Diffusion Filtering Long M (eds) MEDICON (2013) IFMBE Proceedings. Springer, Cham. 2014; pp. 41: 479-82.
- [59] Kamarianakis Z, Buliev I, Pallikarakis N. A platform for Image reconstruction in X-ray Imaging: Medical applications using CBCT and DTS algorithms. *Computer Science Journal of Moldova* 2014; 22(2): 236-54.
- [60] Malliori A, Bliznakova K, Bliznakov Z, Cockmartin L, Bosmans H, Pallikarakis N. Breast tomosynthesis using the multiple projection algorithm adapted for stationary detectors. *J XRay Sci Technol* 2016; 24(1): 23-41. [http://dx.doi.org/10.3233/XST-160538] [PMID: 26890907]
- [61] Malliori A, Bliznakova K, Dermitzakis A, Pallikarakis N. Evaluation of the effect of acquisition parameters on image quality in digital breast tomosynthesis: Simulation studies Long M (eds) WC (2012) IFMBE Proceedings. Springer, Berlin, Heidelberg. 2013; pp. 39: 2211-4.
- [62] Daskalaki A, Bliznakova K, Pallikarakis N. Evaluation of the effect of silicone breast inserts on X-ray mammography and breast tomosynthesis images: A Monte Carlo simulation study *Physica medica : PM : An international journal devoted to the applications of physics to medicine and biology: Official journal of the Italian Association of Biomedical Physics* 2016; 32(2): 353-61.
- [63] Bliznakova K, Speller R, Horrocks J, Liaparinos P, Kolitsi Z, Pallikarakis N. Experimental validation of a radiographic simulation code using breast phantom for X-ray imaging. *Comput Biol Med* 2010; 40(2): 208-14. [http://dx.doi.org/10.1016/j.combiomed.2009.11.017] [PMID: 20056197]
- [64] Bliznakova K, Kolitsi Z, Speller RD, Horrocks JA, Tromba G, Pallikarakis N. Evaluation of digital breast tomosynthesis reconstruction algorithms using synchrotron radiation in standard geometry. *Med Phys* 2010; 37(4): 1893-903. [http://dx.doi.org/10.1118/1.3371693] [PMID: 20443511]
- [65] Malliori A, Bliznakova K, Speller RD, et al. Image quality evaluation of breast tomosynthesis with synchrotron radiation. *Med Phys* 2012; 39(9): 5621-34. [http://dx.doi.org/10.1118/1.4747268] [PMID: 22957628]
- [66] Daskalaki A, Pallikarakis N. Image Quality Evaluation of Phase Contrast Mammographic Techniques. Lhotska, L, Sukupova, L, Lacković, I, Ibbott, G (eds) WC (2018) IFMBE Proceedings. Springer, Singapore. 2019; pp. 68: 9-13.
- [67] Arfelli F, Assante M, Bonvicini V, et al. Low-dose phase contrast x-ray medical imaging. *Phys Med Biol* 1998; 43(10): 2845-52. [http://dx.doi.org/10.1088/0031-9155/43/10/013] [PMID: 9814522]
- [68] Berger MJ, Hubbell JH, Seltzer SM, Chang J, Coursey JS, Sukumar R, et al. XCOM: Photon Cross Section Database (version 15). Gaithersburg, MD: National Institute of Standards and Technology 2010. Available from: <http://physics.nist.gov/xcom>
- [69] Hammerstein GR, Miller DW, White DR, Masterson ME, Woodard HQ, Laughlin JS. Absorbed radiation dose in mammography. *Radiology* 1979; 130(2): 485-91. [http://dx.doi.org/10.1148/130.2.485] [PMID: 760167]
- [70] Crump S. (inventor)Apparatus and method for creating three-dimensional objects US patent US5121329 1992.
- [71] Mohamed O. Optimization of fused deposition modeling process parameters: A review of current research and future prospects. *Advances in Manufacturing* 2015; 3: 42-52. [http://dx.doi.org/10.1007/s40436-014-0097-7]
- [72] Melchels FP, Feijen J, Grijpma DW. A review on stereolithography and its applications in biomedical engineering. *Biomaterials* 2010; 31(24): 6121-30. [http://dx.doi.org/10.1016/j.biomaterials.2010.04.050] [PMID: 20478613]
- [73] Vavrik D, Holy T, Jakubek J, Pospisil S, Vykydal Z, Dammer J. Direct thickness calibration: Way to radiographic study of soft tissues. *Astroparticle, particle and space physics, detectors and medical physics applications* 2006; pp. 773-8.
- [74] Vavrik D, Jakubek J. Radiogram enhancement and linearization using the beam hardening correction method. *Nucl Instrum Methods Phys Res A* 2009; 607(1): 212-4. [http://dx.doi.org/10.1016/j.nima.2009.03.156]
- [75] Procz S, Pichotka M, Lübke J, Hamann E, Ballabriga R, Blaj G, et al. Flat field correction optimization for energy selective X-ray imaging with Medipix3. *IEEE Trans Nucl Sci* 2011; 58(6): 3182-9. [http://dx.doi.org/10.1109/TNS.2011.2165732]
- [76] Wu S, Yu S, Yang Y, Xie Y. Feature and contrast enhancement of mammographic image based on multiscale analysis and morphology. *Comput Math Methods Med* 2013; 2013716948.
- [77] Sickles E, D'Orsi C, Bassett L. ACR BI-RADS® Mammography ACR BI-RADS® Atlas, Breast Imaging Reporting and Data System. Reston, VA: American College of Radiology 2013.